Journal of Aerospace Technology and Management
ISSN: 1984-9648
editor@jatm.com.br
Instituto de Aeronáutica e Espaço
Brasil

R. Wolf, William; K. Lele, Sanjiva
Fast Multipole Burton-Miller Boundary Element Method for Two and Three-Dimensional Acoustic Scattering
Journal of Aerospace Technology and Management, vol. 4, núm. 2, abril-agosto, 2012, pp. 145-161
Instituto de Aeronáutica e Espaço
São Paulo, Brasil

doi: 10.5028/jatm.2012.04021812

Fast Multipole Burton-Miller Boundary Element Method for Two and Three-Dimensional Acoustic Scattering

William R. Wolf[1,2,*], Sanjiva K. Lele[1]
[1]Stanford University - Stanford/CA – USA
[2]Instituto de Aeronáutica e Espaço - São José dos Campos/SP – Brazil

Abstract: *A multistage adaptive fast multipole method is used to accelerate the matrix-vector products arising from the Burton-Miller boundary integral equations, which are formed in a boundary element method. The present study considers the scattering of acoustic waves, generated by localized sources from bodies with rigid surfaces. Details on the implementation of a multistage adaptive fast multipole method are described for two and three-dimensional formulations. The code is verified through the solution of well documented test cases. The fast multipole method is tested for acoustic scattering problems of single and multiple bodies, and a discussion is provided on the performance of the method. Results for engineering problems with complex geometries, such as a multi-element wing, are presented in order to assess the implemented capability.*

Keywords: *Fast Multipole Method, Boundary Element Method, Burton-Miller Formulation, Acoustic Scattering.*

INTRODUCTION

The development of physics-based noise prediction tools for analyzing aerodynamic noise sources, such as the jet and airframe ones, is of paramount importance, since noise regulations have become more stringent, and more sophisticated methods are needed to achieve the required noise reductions without a significant performance penalty. The design of 3D complex configurations requires the use of time-consuming numerical simulations for the study and mitigation of noise sources. In the context of aeroacoustics, several acoustic scattering codes, such as the fast scattering code (FSC) from NASA Langley Research Center (Dunn and Tinetti, 2004; 2005; Tinetti *et al*., 2007, Dunn and Farassat, 2007) and the ACTI3S and the ACTIPOLE codes from Airbus-F, (Delnevo *et al*., 2005), are under development. These scattering codes solve the Helmholtz equation through the discretization of boundary integral equations by the boundary element method (BEM) or by the equivalent source method (ESM). It is found that the fast multipole method (FMM) accelerates the computations of BEM and ESM formulations leading to high improvements in simulation time and memory storage (Nishimura, 2002; Sakuma and Yasuda, 2002; Chen and Chen, 2003; Darve and Have, 2004). In the present work, we have developed a scattering code for 2D and 3D simulations using a multilevel FMM and BEM. In the future, the code will be used for the analysis of airframe noise sources and for exploring strategies for their mitigation.

The use of BEM for solving scattering and radiation problems in acoustics provides several advantages over finite element methods (FEM) and finite difference methods (FDM). Among these, one can cite the advantage of requiring only the boundary discretization, simplified preprocessing, and accurate modeling of infinite domains. However, for large scale problems, the solution of the nonsymmetric dense matrices appearing in the BEM have computational complexity proportional to $O(n^2)$ when an iterative solver is used, which makes the method prohibitive to use. Here, n is the number of boundary elements used in the discretization. In order to reduce the computational complexity, one can use FMM to accelerate the solution of the linear systems and reduce the computational complexity to an order proportional to $O(n \log n)$.

The FMM was introduced by Rokhlin (1983) for the solution of integral equations of classical potential theory. However, the method was further developed and became famous for the solution of N−body problems in the paper of Greengard and Rokhlin (1987).

Received: 26/03/12 Accepted: 26/04/12
*author for correspondence: willwolf@gmail.com
Pç. Mal. Eduardo Gomes, 50. CEP: 12.228-901
São José dos Campos/SP – Brazil

The application of the FMM for acoustic scattering was introduced by Rokhlin (1990) for the solution of integral equations of scattering theory in 2D. Since then, the FMM has been used to accelerate the solution of BEM in several studies of acoustic scattering in 2D and 3D, and different approaches were developed based on the range of frequencies analyzed (Nishimura, 2002; Sakuma and Yasuda, 2002; Chen and Chen, 2003; Darve and Have, 2004; Cheng *et al*., 2006; Shen and Liu, 2007; Wolf and Lele, 2010).

While the approach proposed by Rokhlin (1990) is considered a single stage or two-level FMM, which provides computational complexity proportional to O($n^{4/3}$), the methods that appeared in Nishimura (2002), Sakuma and Yasuda (2002), Chen and Chen (2003), Darve and Have (2004), Cheng *et al*. (2006), Shen and Liu (2007) and Wolf and Lele (2009) are multilevel FMM and have computational complexity O(n log n). In the direct BEM, large nonsymmetric dense linear systems are formed by the discretization of the boundary integrals. The FMM accelerates the matrix-vector products in the iterative solutions of the large-scale linear systems, without composing the dense influence coefficient matrices used in the direct BEM.

In the present work, we have studied the sound scattering from rigid bodies induced by localized sources. The Burton-Miller equation is solved using a BEM formulation, whose numerical solution is accelerated by a multilevel adaptive FMM (Nishimura, 2002; Wolf and Lele, 2009; Cheng *et al*., 1999; Yoshida, 2001). The conjugate gradient squared – CGS (Sonneveld, 1989) iterative solver is used to perform the matrix-vector products in the linear systems formed by the boundary integral equations. Several FMM formulations are described in the literature for the solution of the Burton-Miller boundary integral equation (Li and Huang, 2011; Wu *et al*., 2011; Wu *et al*., 2012). The methods applied in these references make use of diagonal formulations, which provide higher acceleration of BEM linear systems for high frequencies. However, as described in literature (Nishimura, 2002; Wolf and Lele, 2009), these formulations are unstable at low frequencies due to the sub-wavelength breakdown. The current FMM formulation is stable for any range of frequencies and can be further accelerated by the method described in Wolf and Lele (2009).

In the work carried out by Li and Huang (2011), a modified Burton-Miller formulation was presented in order to avoid the solution of hyper-singular integrals appearing in the BEM. In the present work, these hyper-singular integrals are solved using a method that is easy to implement for any singular kernel and that allows one to use regular Gaussian quadrature. Numerical tests are performed to assess the capability implemented. The sound scattering of sound from localized axisymmetric cylindrical and spherically symmetric sources by a cylinder and a sphere is computed and compared with the corresponding analytical solutions. Benchmark comparisons between the direct BEM and the adaptive FMM and BEM are presented. The complete 2D and 3D FMM formulations are presented with details on the implementation of the adaptive multilevel FMM. Also, additional results of low frequency acoustic scattering by complex geometries, *e.g.*, a cylinder with a cavity, multiple cylinders and spheres, and a multielement wing are analyzed.

THEORETICAL FORMULATION

The scattering of sound waves produced by a spatial distribution of concentrated sources is solved in the present paper. The following non-homogeneous Helmholtz equation represents the pressure disturbances induced by concentrated sources in a homogeneous medium, with zero mean flow

$$\nabla^2 p(\vec{x}) + k^2 p(\vec{x}) = -Q_{si}\delta(\vec{x} - \vec{x}_{si}). \tag{1}$$

In Eq. 1, p represents the pressure, k is the wave number, Q_{si} represents the *i-th* source strength, $\vec{x}$ is a field point, and $\vec{x}_{si}$ is the *i-th* source location. The convention e^{-iwt} is assumed for time dependence. A fundamental solution for the Helmholtz equation is the free space Green function, $G(\vec{x}, \vec{y})$, which is represented by Eq. 2:

$$G(\vec{x},\vec{y}) = \frac{i}{4}H_0^{(1)}(k|\vec{x} - \vec{y}|), \tag{2}$$

for a 2-D formulation, or Eq. 3,

$$G(\vec{x},\vec{y}) = \frac{e^{ik|\vec{x}-\vec{y}|}}{4\pi|\vec{x} - \vec{y}|}, \tag{3}$$

for a 3D formulation. Here, $H_0^{(1)}$ stands for the Hankel function of the first kind and order zero. Therefore, one can write the Helmholtz equation for the particular solution given by the Green function as Eq. 4:

$$\nabla^2 G(\vec{x},\vec{y}) + k^2 G(\vec{x},\vec{y}) = -\delta(\vec{x} - \vec{y}). \tag{4}$$

Using Green's second identity with Equations 1 and 4, one can write the boundary integral equation in Eq. 5:

$$c(\vec{x})p(\vec{x}) = \int_S \left[\frac{\partial p(\vec{y})}{\partial n_y} G(\vec{x},\vec{y}) - \frac{\partial G(\vec{x},\vec{y})}{\partial n_y}\right] dS - \sum_{i=1}^{N\ sourses} Q_{si} G(\vec{x},\vec{x}_{si}), \quad (5)$$

where, $c(\vec{x})$ is equal to 1/2, when $\vec{x}$ is on a smooth boundary surface S and $c(\vec{x})$ is equal to 1 when $\vec{x}$ is a field point.

The derivatives with respect to the inward normal direction of the boundary surface are represented by $\frac{\partial(.)}{\partial n}$ and $\vec{n}$ is an inward unit normal. Figure 1 shows a sketch of an acoustic field with scattering body S and source location X_{si}. The term S_{inf} represents a surface far from the scattering body. The boundary conditions specified on the surface of the scatterer can represent an acoustic rigid surface, $\frac{\partial p}{\partial n} = 0$, or a reacting surface, $\frac{\partial p}{\partial n} = iw\rho p/Z(w)$. However, in the present work, only rigid surfaces are considered. In these boundary conditions, ω is the angular frequency, ρ is the density of the medium, and Z is the acoustic impedance. One should note that the Sommerfeld's radiation condition, which allows only solutions with outgoing waves at infinity to be admitted, $\left(\frac{\partial p}{\partial n} - ikp = 0\right)_\infty$, is naturally satisfied for the BEM formulation on S_{inf}.

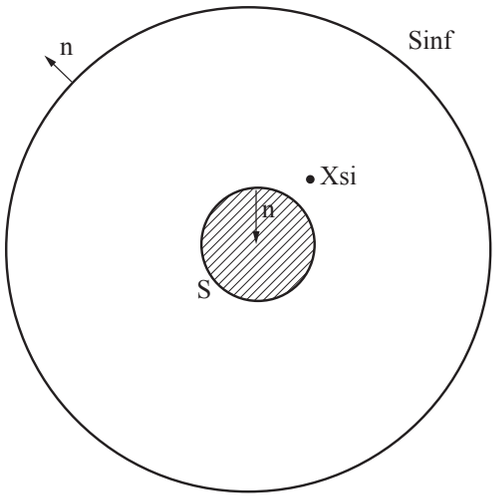

Figure 1. Sketch of acoustic field with scattering body and source location.

Equation 5 represents a fundamental formulation for acoustic analysis in the BEM. However, the solution for this integral formulation of the Helmholtz problem for external acoustic wave problems is non-unique for the so-called forbidden frequencies. This non-uniqueness has no physical meaning, it is a drawback of the mathematical formulation (Burton and Miller, 1971). Several boundary integral formulations have been proposed to overcome this problem (Jones, 1974; Piaszczyk and Klosner, 1984), and the combined Helmholtz integral equation formulation –CHIEF (Schenck, 1968) and the Burton-Miller formulation (Burton and Miller, 1971) are the most widely used methods. The CHIEF method presents some instability problems (Seybert and Rengarajan, 1987), depending on the number and location of sources and, therefore, in this paper, the Burton-Miller method is implemented since it is valid for any problem configuration. The Burton-Miller formulation (Burton and Miller, 1971) considers a complex linear combination of the standard integral equation, Eq. 5, with a hyper-singular integral equation, resulting in Eq. 6:

$$\begin{aligned} c(\vec{x})p(\vec{x}) + \alpha c(\vec{x})\frac{\partial p(\vec{y})}{\partial nx} &= \int_S \left[\frac{\partial p(\vec{y})}{\partial ny} G(\vec{x},\vec{y}) - \frac{\partial G(\vec{x},\vec{y})}{\partial ny} p(\vec{y})\right] dS \\ &- \sum_{i=1}^{N\ sourses} Q_{si} G(\vec{x},\vec{x}_{si}) + \alpha \int_S \left[\frac{\partial p(\vec{y})}{\partial n_y}\frac{\partial G(\vec{x},\vec{y})}{\partial n_x} - \frac{\partial^2 G(\vec{x},\vec{y})}{\partial n_x \partial n_y} p(\vec{y})\right] dS. \\ &- \alpha \sum_{i=1}^{N\ sourses} Q_{si} \frac{\partial G(\vec{x},\vec{x}_{si})}{\partial n_x} \end{aligned} \quad (6)$$

In Eq. 6, the terms $\frac{\partial(.)}{\partial n_x}$ and $\frac{\partial(.)}{\partial n_y}$ represent normal derivatives computed at points $\vec{x}$ and $\vec{y}$, respectively, and α, which must be an imaginary number (Burton and Miller, 1971), was chosen as i/k in the present work.

In the general BEM formulation, the scattering surface, S, is discretized into a finite number of elements with polynomial reconstructions for the unknown inside each element. Then, a boundary integral equation, such as Eq. 6, is solved for each of these elements through the solution of a generally non-symmetric dense linear system of equations, $[A]\{p\}=\{Q\}$. In this linear system, the known boundary values or the known sources appear as the forcing term, $\{Q\}$, as in Eq. 7:

$$\begin{bmatrix} a_{11} & a_{12} & \cdots & a_{1N} \\ a_{21} & a_{22} & \cdots & a_{2N} \\ \vdots & \vdots & \cdots & \vdots \\ a_{N1} & a_{N2} & \cdots & a_{NN} \end{bmatrix} \begin{Bmatrix} p_1 \\ p_2 \\ \vdots \\ p_N \end{Bmatrix} = \begin{Bmatrix} -\sum_{i=1}^{N\ sourses} Q_{si}(G(\vec{x}_1,\vec{x}_{si}) + \alpha \frac{\partial G(\vec{x}_1,\vec{x}_{si})}{\partial n_1} \\ -\sum_{i=1}^{N\ sourses} Q_{si}(G(\vec{x}_2,\vec{x}_{si}) + \alpha \frac{\partial G(\vec{x}_2,\vec{x}_{si})}{\partial n_2} \\ \vdots \\ -\sum_{i=1}^{N\ sourses} Q_{si}(G(\vec{x}_N,\vec{x}_{si}) + \alpha \frac{\partial G(\vec{x}_N,\vec{x}_{si})}{\partial n_N} \end{Bmatrix}. \quad (7)$$

For a rigid surface, the coefficients of matrix $[A]$ are given by $a_{ij} = 1/2\delta_{ij} + \int_S \frac{\partial G(\vec{x}_i,\vec{x}_j)}{\partial n_j} + \alpha \frac{\partial^2 G(\vec{x}_i,\vec{x}_j)}{\partial n_i \partial n_j} dS$, where ∂_{ij} is the Kronecker delta.

The matrix-vector products involving the unknowns are solved by an iterative solver (CG, CGS, GMRES) or a direct method (Gaussian elimination). In the present work, polynomial reconstructions for the elements considered in the BEM formulation are of the constant type, which makes the implementation of the FMM easier, avoid discontinuous fluxes on the nodes of the elements, and simplify the solutions of the singular integrals in Eq. 6. In order to solve the system of equations, we use the CGS (Sonneveld, 1989) iterative solver,

and an adaptive FMM is used to accelerate the matrix-vector calculations in the linear systems. While the FMM method is used for far-field interactions among elements, near-field interactions are computed with direct computations using the BEM. Therefore, we have to solve the singular integrals appearing in the Burton-Miller BEM formulation.

Several approaches are found in the literature on how to compute BEM singular integrals for acoustics, mainly for hyper-singular integrals (Chien *et al*., 1990; Liu *et al*., 1992; Geng *et al*., 1996). In this paper, we present a method that is easy to implement for any singular kernel and that allows one to use regular Gaussian quadrature. We first divide the boundary elements into smaller triangular elements, as shown in Fig. 2, and perform a transformation from Cartesian to polar coordinates. The transformed singular integrals will have the form as in Eq. 8:

$$\int_S \frac{f(\vec{x},\vec{y})}{|\vec{x}-\vec{y}|^n} dS = \int_S \frac{f(R,\theta)}{R^{n-1}} dR d\theta, \tag{8}$$

They will be weakly singular for n=1, strongly singular for n=2, and hyper-singular for n=3. The weakly singular integrals can be solved with regular Gaussian quadrature integration, since, after the transformation, the singular kernel vanishes. The strongly singular and hyper-singular kernels are solved in the radial direction in their Cauchy and Hadamard finite part sense following the work of Brandão (1987). The equations are worked out here for the specific case when the singular point lies at one of the limits of integration.

$$\begin{aligned}
&\int_0^{\theta\max} F.P \int_0^{R(\theta)} \frac{f(R)}{R^{n-1}} dR d\theta \\
&= \int_0^{\theta\max} \int_0^{R(\theta)} \frac{\left[f(R) + \sum_{j=0}^{n-2} \frac{(-1)^{j+1}}{j!} f^{(j)}|_{R=0} (-R)^j \right]}{R^{n-1}} dR \\
&- \int_0^{\theta\max} \sum_{j=0}^{n-2} \frac{(-1)^{2j+1}}{j!} f^{(j)}|_{R=0} \left[F.P. \int_0^{R(\theta)} \frac{1}{R^{n-1-j}} \right] dR.
\end{aligned} \tag{9}$$

In Eq. 9, the finite part integrals in the last term are given by $F.P. \int_0^{R(\theta)} \frac{1}{R^{n-1-j}} dR = \frac{(-1)^{n-2}}{(n-2) R(\theta)^{n-2}}$ for n=3 or higher and $F.P. \int_0^{R(\theta)} \frac{1}{R^{n-1-j}} dR = ln(R(\theta))$ for n=2. The function $f = e^{(ikR(\theta))}$ and $f^{(j)}$ is the $j-th$ derivative of f. One should note that the term R depends on θ, $R(\theta) = \frac{R_0 sin\beta}{sin(\pi - \beta - \theta)}$, and the integrals are computed simultaneously in both variables. Following this method, all the singular integrals can be computed by regular Gaussian quadrature formulae and without any regularization procedure.

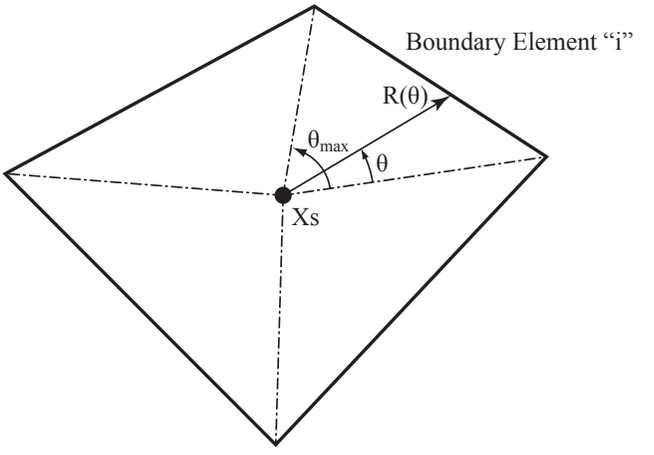

Figure 2. Element subdivision performed for the singular integration around the singular point Xs.

FAST MULTIPOLE METHOD

The adaptive FMM implemented in this work follows the ideas from Carrier *et al*. (1988) and Nishimura (2002), for the 2D formulation, and from Cheng *et al*. (1999), Yoshida (2001) and Shen and Liu (2007), for the 3D one. It consists of clustering boundary elements at different spatial lengths and using multipole expansions to evaluate the interactions among clusters, which are well-separated from each other. We define two well-separated clusters as sets of elements that are circumscribed by circles in 2D or spheres in 3D and whose centroids are distant from each other by a length of at least three times their radius. One can improve accuracy by increasing this parameter. However, this will reduce the performance of the method because more direct BEM computations will be performed. The nearby elements are computed by the direct solution of the boundary integral equations as in any typical BEM formulation. In the accelerated BEM, the surface boundary is discretized into elements and the entire boundary object is surrounded by a square in 2D or a cube in 3D, which is the computational box. Then, a recursive algorithm for the refinement of the computational box is applied in order to form the different expansion levels for the FMM. The recursive algorithm presented here performs an adaptive refinement of the computational box for all box levels, and it works for both 2D and 3D FMM, independent of the formulations employed for multipole expansions and translations. In this section, the algorithm is presented for a 2D FMM formulation; however, the 3D approach follows the same methodology, except that one should replace the quad-tree structures by oct-tree ones.

When the FMM algorithm starts, the entire computational box is at level 0 and surrounds the scattering body of interest, which is discretized by boundary elements. The general idea consists of refining the computational box into four smaller boxes, which will be at level 1 and inspecting the number of elements contained by each of the new boxes. This process continues until the number of boundary elements inside all boxes is smaller than or equal to a certain prescribed number. In Fig. 3, one can observe a computational box surrounding an airfoil with all the smaller boxes showing the adaptive refinement in regions where the number of boundary elements exceeds the maximum allowed per box. This prescribed number of elements per box will define the maximum stage in the FMM. Boxes of level l+1 are children of the parent boxes of level l. Each parent box is divided into four children and these are direct neighbors among themselves, which means that they share a common node or edge. Following the algorithm, one can write a quad-tree structure containing all children from all boxes, at all levels. At every level of refinement, a table of nonempty boxes is maintained, so that once an empty box is encountered, its existence is forgotten and it is not used in the subsequent process.

In order to implement the FMM, we define a set of lists containing some specific boxes, such as direct and parent neighbors, among others. These lists will help with the computation of multipole expansions and translations and the acceleration of the FMM. List L_1 of a box b consists of box b itself and all boxes that do not contain children boxes and that share a node or edge with b. If b is a parent box, then $L_1 = \emptyset$. List L_2 of a box b is the iterative list from the original FMM (Greengard and Rokhlin, 1987), and it consists of all children of b parent neighbors, which are well-separated from it. List L_3 is empty if b is a parent box, and it consists of all children of b neighbors, at any level, which do not share a node or vertex with b. Finally, list L_4 of box b is formed by all boxes c, such as that $b \in L_3(c)$. It is possible to see that all boxes in $L_3(b)$ are at higher levels than b, *i.e.*, are smaller than b, and all boxes in $L_4(b)$ are at smaller levels than b, *i.e.*, they are larger than b. Beyond that, all boxes in $L_4(b)$ do not have children. In Fig. 4, one can observe the lists associated with a box b. In this figure, all boxes are marked with numbers corresponding to the respective lists that they are associated with. The boxes marked with number five are those well-separated from b parent, which means that they are in L_2 (b parent) or L4 (b parent). The authors suggest the papers from Cheng *et al*. (1999) and Nishimura (2002) and the thesis from Yoshida (2001) for a more detailed explanation on the FMM implementation, including the adaptive refinement procedure and the several steps described in the following paragraphs.

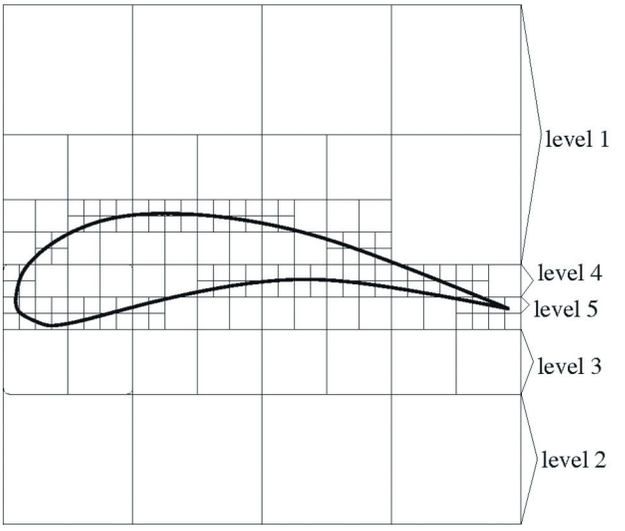

Figure 3. Different box levels of the adaptive refinement.

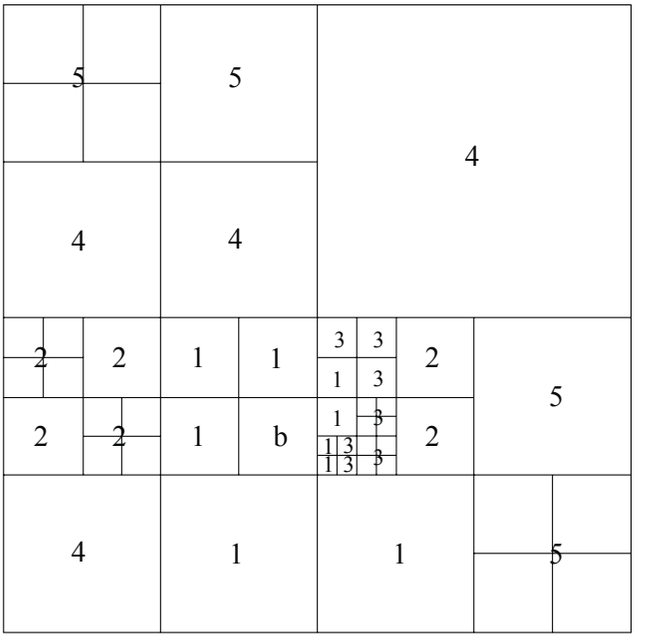

Figure 4. Associated lists of box b.

The FMM is often applied to integral or summation equations, which contain degenerate kernels. The Green function, $G(x,y)$ in Eqs. 5 and 6 is the degenerate kernel one wants to expand in a suitable form in order to apply the FMM. Instead of computing the influence of all source elements at $\vec{y}$ to all field elements at $\vec{x}$ directly, one can write the Green function as in Eq. 10:

$$G(\vec{x},\vec{y}) = \sum_i k_i^{(1)}(\vec{x}-\vec{z})k_i^{(2)}(\vec{y}-\vec{z}), \tag{10}$$

and, then, compute multipole approximations representing the acoustic field of the far away elements by clusters of elements.

Thus, the first step in the FMM algorithm consists of computing all the multipole expansions around the centroids of all childless boxes, represented by $\vec{z}$ in Eq. 10. Using Eq. 10, which holds for distances $|\vec{x}-\vec{z}|$ larger than $|\vec{y}-\vec{z}|$, one can write the multipole expansions for Eq. 6 as Eq. 11:

$$M_i(\vec{z}) = \int_{S_0}\left[\frac{\partial p(\vec{y})}{\partial n_y}k_i^{(2)}(\vec{y}-\vec{z}) - \frac{\partial k_i^{(2)}(\vec{y}-\vec{z})}{\partial n_y}p(\vec{y})\right]dS, \qquad (11)$$

where, S_0 is a set of discrete elements inside the box with centroid $\vec{z}$. Each element inside the box is represented in a multipole expansion and all the multipoles are summed to form a total representation of the sources inside the box. This step is represented as "Step 1" in Fig. 5.

Subsequently, all the multipole expansions from the childless boxes at all levels are shifted to the centroids of their parent boxes up to level 2. Thus, we have multipole expansions for the boxes in level 2 representing their influence on the field outside each box. The translation of multipoles from centroids of boxes of level l+1 to their parents centroids at level l is commonly called multipole-to-multipole (M2M) translation or upward pass, and it can be seen in "Step 2" in Fig. 5. In the next step, which is represented in Fig. 5 as "Step 3", the multipole expansions for the boxes in L_2(b) are converted to local expansions about b centroid and added up forming a local expansion around b centroid, representing the field of the elements from the well-separated boxes at the same level of b. Following the same ideas, the multipole expansions for the boxes in L_4(b) are converted to local expansions about b centroid and added up. These conversions from multipoles to local representations around centroids of well-separated boxes are frequently called multipole-to-local (M2L) expansions in the literature. All the local representations from L_2 and L_4 are then shifted to b children, until the highest refinement level is reached. One can observe these calculations in "Step 4" of Fig. 5, which is referred in the literature as local-to-local (L2L) translation or downward pass.

Finally, all the calculations can be performed in order to represent the influence of far-field sources to each of the boundary elements. In Fig. 5, one can observe this type of calculation in "Step 5", in which the local coefficients computed for the centroids of the boxes in the highest level of refinement are used to compute the effects of far-field sources to each of the elements contained inside box b. Once the influence of the far elements is considered, a further step includes the evaluation of nearby elements influence. For each childless box b, we compute the direct interactions among all elements inside b and those on $L_1(b)$ and $L_3(b)$. All the interactions from elements on $L_1(b)$ are calculated using direct BEM formulations, since they cannot be expanded in multipoles. However, for $L_3(b)$, we compute multipole expansions for all elements inside the boxes in $L_3(b)$, and, then, compute the effects of these multipoles to each of the elements inside b. These near-field calculations can be observed in "Step 6" of Fig. 5.

All theorems and analytical tools, which prove the validity of the multipole expansions and translations, and several formal analysis of accuracy and algorithm complexity for the FMM are available in literature (Greengard and Rokhlin, 1987; Carrier *et al*., 1988; Epton and Dembart, 1995; Labreuche, 1998; Darve, 2000).

Other FMM formulations for low-frequency scattering can also be found in the works from Darve and Have (2004), Sakuma and Yasuda (2002 a, b) and Gumerov and Duraiswami (2003). In the former methods, the authors computed the multipole expansions and translations using plane wave expansions and in the latter, Gumerov and Duraiswami (2003) used a formulation similar to the one used in the present work plus recursive relations of the translation operators and rotation-coaxial translation decomposition of the translation operators to reduce the computational complexity of the algorithm. These methods will be studied in a future work and they are beyond the scope of the present paper.

2D Formulation

In this subsection, for the sake of completeness, we present the formulations used for the 2D algorithm. These equations are well-documented in Nishimura (2002). Equation 2 can be written as an expansion of the degenerate kernels such as in Eq. 12:

$$G(\vec{x},\vec{y}) = \frac{i}{4}\sum_{n=-\infty}^{\infty} O^n(\overrightarrow{ox})I^{-n}(\overrightarrow{oy}), \qquad (12)$$

where the functions O^n and I^n are defined as Eqs. 13 and 14:

$$O^n(\vec{X}) = i^n H_n^{(1)}(kr)e^{in\theta} \qquad (13)$$

and

$$I^n(X) = (-i)^n J_n(kr)e^{in\theta}. \qquad (14)$$

In the last expression, J_n stands for the $n-th$ order Bessel function of the first kind and r and θ are the polar

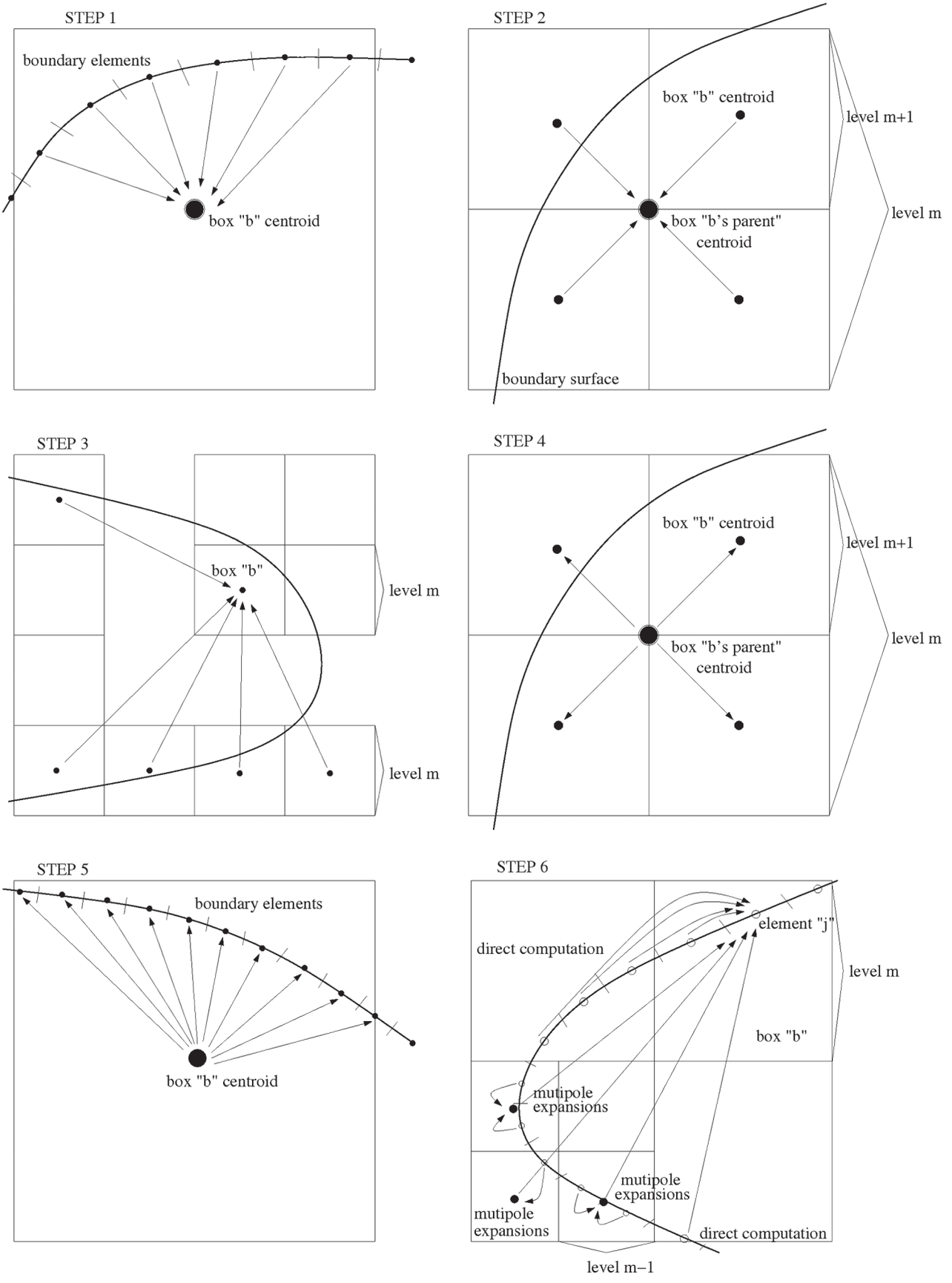

Figure 5. Schematic diagram for the several steps in the fast multipole method.

coordinates of some vector $\overrightarrow{X}$, which can be $\overrightarrow{ox}$ or $\overrightarrow{oy}$, for instance. The vectors $\overrightarrow{ox}$ and $\overrightarrow{oy}$ point from some box center, $\vec{o}$, to a far-field source location, $\vec{x}$, and a near-field one, $\vec{y}$, respectively. To have a good approximation in Eq. 12 one should truncate the series using p terms, where $p > k|\overrightarrow{oy}|$. Thus, the boundary integrals appearing in Eq. 6 can be written as Eqs. 15 and 16:

$$\int_{S_0}\left[\frac{\partial p(\vec{y})}{\partial n_y}G(\vec{x},\vec{y})-\frac{\partial G(\vec{x},\vec{y})}{\partial n_y}p(\vec{y})\right]dS=\frac{i}{4}\sum_{n=-\infty}^{\infty}O^n(\overrightarrow{ox})M_{-n}(\vec{o}) \quad (15)$$

and

$$\int_{S_0}\left[\frac{\partial p(\vec{y})}{\partial n_y}\frac{\partial G(\vec{x},\vec{y})}{\partial n_x}-\frac{\partial^2 G(\vec{x},\vec{y})}{\partial n_x\partial n_y}p(\vec{y})\right]dS=\frac{i}{4}\sum_{n=-\infty}^{\infty}\frac{\partial O^n(\overrightarrow{ox})}{\partial n_x}M_{-n}(\vec{o}) \quad (16)$$

Therefore, following the notation from Eq. 11, one can write multipole expansions Mn ($\vec{o}$) as Eq. 17:

$$M_n(\vec{o})=\int_{S_0}\left[\frac{\partial p(\vec{y})}{\partial n_y}I^n(\overrightarrow{oy})-\frac{\partial I^n(\overrightarrow{oy})}{\partial n_y}p(\vec{y})\right]dS. \quad (17)$$

In Eq. 17, it is assumed that the origin $\vec{o}$ is located closely to the boundary element S_0 and, then, $|\overrightarrow{ox}| > max|\overrightarrow{oy}|$ holds.

The M2M (Eq. 18), M2L (Eq. 19) and L2L (Eq. 20) expansions and translations are given by Eqs. 18 to 20:

$$M_n(\vec{o}')=\sum_{v=-\infty}^{\infty}I^{n-v}(\overrightarrow{o'o})M_v(\vec{o}), \quad (18)$$

$$L_n(\vec{o}')=\sum_{v=-\infty}^{\infty}O^{n-v}(\overrightarrow{oo'})M_v(\vec{o}), \quad (19)$$

$$L_n(\vec{o}')=\sum_{v=-\infty}^{\infty}I^{n-v}(\overrightarrow{o'o})L_v(\vec{o}). \quad (20)$$

In Eq. 18, $\vec{o}'$ is the center of a parent box and $\vec{o}$ is the center of one of its children, and in Eqs. 19 and 20, $\vec{o}$ is assumed to be closer to $\vec{x}$ compared to $\vec{o}'$. Finally, we can also write the boundary and hyper-singular integral equations as functions of the local expansions (Eqs. 21 and 22):

$$\int_{S_0}\left[\frac{\partial p(\vec{y})}{\partial n_y}G(\vec{x},\vec{y})-\frac{\partial G(\vec{x},\vec{y})}{\partial n_y}p(\vec{y})\right]dS=\frac{i}{4}\sum_{n=-\infty}^{\infty}(-1)^n I^n(\overrightarrow{o'x})L_{-n}(\vec{o}') \quad (21)$$

and

$$\int_{S_0}\left[\frac{\partial p(\vec{y})}{\partial n_y}\frac{\partial G(\vec{x},\vec{y})}{\partial n_y}-\frac{\partial^2 G(\vec{x},\vec{y})}{\partial n_x\partial n_y}p(\vec{y})\right]dS=\frac{i}{4}\sum_{n=-\infty}^{\infty}(-1)^n\frac{\partial I^n(\overrightarrow{o'x})}{\partial n_x}L_{-n}(\vec{o}'). \quad (22)$$

3D Formulation

For the same reason as in the previous subsection, we present the formulations used for the 3D algorithm. These equations are well-documented in Yoshida (2001). Equation 3 can be written as an expansion of degenerate kernels such as Eq. 23:

$$G(\vec{x},\vec{y})=\frac{ik}{4\pi}\sum_{n=0}^{\infty}(2n+1)\sum_{m=-n}^{n}O_n^m(\overrightarrow{ox})\overline{I_n^m}(\overrightarrow{oy}) \quad (23)$$

where the function O_m^n is defined as Eq. 24

$$O_n^m(\vec{X})=h_n^{(1)}(kr)Y_n^m(\theta,\phi) \quad (24)$$

and $\overline{I_n^m}$ is the complex conjugate of I_n^m, defined as Eq. 25

$$I_n^m(\vec{X})=j_n(kr)Y_n^m(\theta,\phi). \quad (25)$$

In these expressions, j_n represents the *n-th* order spherical Bessel function of the first kind, $h_n^{(1)}$ is the *n-th* order spherical Hankel function of the first kind and $\mathrm{Y_n^m}$ are the spherical harmonics defined as Eq. 26:

$$Y_n^m(\theta,\phi)=\sqrt{\frac{(n-m)!}{(n+m)!}}P_n^m(\cos\theta)e^{im\phi}, \quad (26)$$

where P_n^m stands for the associated Legendre functions. The terms r, θ, ϕ represent the spherical coordinates of some vector $\vec{\mathrm{X}}$, which can be $\overrightarrow{ox}$ or $\overrightarrow{oy}$, for instance. The vectors $\overrightarrow{ox}$ and $\overrightarrow{oy}$ point from some box center, $\vec{o}$, to a far-field source location, $\vec{x}$, and a near-field source location, $\vec{y}$, respectively. Again, in Eq. 23, $|\overrightarrow{ox}| > max|\overrightarrow{oy}|$ holds. The boundary integrals in Eq. 6 can be written as Equations 27 and 28:

$$\int_{S_0}\left[\frac{\partial p(\vec{y})}{\partial n_y}G(\vec{x},\vec{y})-\frac{\partial G(\vec{x},\vec{y})}{\partial n_y}p(\vec{y})\right]dS=\frac{ik}{4\pi}\sum_{n=0}^{\infty}(2n+1)\sum_{m=-n}^{n}O_n^m(\overrightarrow{ox})M_n^m(\vec{o}) \quad (27)$$

and

$$\int_{S_0}\left[\frac{\partial p(\vec{y})}{\partial n_y}\frac{\partial G(\vec{x},\vec{y})}{\partial n_x}-\frac{\partial^2 G(\vec{x},\vec{y})}{\partial n_x\partial n_y}p(\vec{y})\right]dS=\frac{ik}{4\pi}\sum_{n=0}^{\infty}(2n+1)\sum_{m=-n}^{n}\frac{\partial O_n^m(\overrightarrow{ox})}{\partial n_x}M_n^m(\vec{o}). \quad (28)$$

Therefore, following the notation from Eq. 11, one can write multipole expansions $M_n^m(\vec{o})$ as in Eq. 29:

$$M_n^m(\vec{o})=\int_{S_0}\left[\frac{\partial p(\vec{y})}{\partial n_y}\overline{I_n^m}(\overrightarrow{oy})-\frac{\partial\overline{I_n^m}(\overrightarrow{oy})}{\partial n_y}p(\vec{y})\right]dS. \quad (29)$$

The M2M (Eq. 30), M2L (Eq. 31) and L2L (Eq. 32) expansions and translations are given by Eqs. 30 to 32:

$$M_n^m(\vec{o}') = \sum_{n'=0}^{\infty} \sum_{m'=-n'}^{n'} \sum_{l=|n-n'|}^{n+n'} (2n'+1)(-1)^{m'} W_{n,n',m,m',l}\, I_l^{-m-m'}(\overrightarrow{o'o})\, M_n^{-m'}(\vec{o}) \quad (30)$$

$$L_n^m(\vec{o}') = \sum_{n'=0}^{\infty} \sum_{m'=-n'}^{n'} \sum_{l=|n-n'|}^{n+n'} (2n'+1) W_{n',n,m',m,l}\, \tilde{O}_l^{-m-m'}(\overrightarrow{oo'})\, M_{n'}^{m'}(\vec{o}) \quad (31)$$

$$L_n^m(\vec{o}') = \sum_{n'=0}^{\infty} \sum_{m'=-n'}^{n'} \sum_{l=|n-n'|}^{n+n'} (2n'+1)(-1)^{m} W_{n',n,m',-m,l}\, I_l^{m-m'}(\overrightarrow{oo'})\, L_{n'}^{m'}(\vec{o}) \quad (32)$$

In Eq. 30, $\vec{o}'$ is the center of a parent box and $\vec{o}$ is the center of one of its children, and in Eqs. 31 and 32, $\vec{o}'$ is assumed to be closer to $\vec{x}$ compared to $\vec{o}$. For all these expressions, the summations in l, $\sum_{l=|n-n'|}^{n+n'}$ are performed only for even values of $n+n'-l$. Also in these formulas, the term $\widetilde{O_n^m} = h_n^{(1)}(kr)\,\overline{Y_n^m}(\theta,\phi)$, and the term $W_{n,n',m,m',l}$ are computed using the formula in Eq. 33:

$$W_{n,n',m,m',l} = (2l+1)\, i^{n'-n+l} \begin{pmatrix} n & n' & l \\ 0 & 0 & 0 \end{pmatrix} \begin{pmatrix} n & n' & l \\ m & m' & t \end{pmatrix} \quad (33)$$

where, $t=-m-m'$ and $\begin{pmatrix} a & b & c \\ d & e & f \end{pmatrix}$ denotes the Wigner 3j symbol, which can be computed using the Racah formula (Messiah, 1987).

RESULTS

The present section presents results obtained by the BEM accelerated by the adaptive FMM. The problems analyzed include a 2D cylinder, a sphere, 2D and 3D cylinders with and without cavities, multiple spheres, and a 3D multi-element wing.

Code verification

The first problem of interest considers the acoustic scattering around a 2D rigid cylinder due to a localized axisymmetric cylindrical source. The solution for such problem is compared with the analytical one presented by Morris (1995). The problem is described by a point source placed at a distance L from the center of the cylinder. In the present computations, the distance L=1.0 m, the radius of the cylinder is set a=0.5 m, and the wave number is k=10 m^{-1}, which corresponds to a frequency of f=541.4 *Hz* for a speed of sound c=340.0 ms^{-1}.

For this test problem, the boundary of the cylinder is discretized by four different meshes consisting of 1,000, 1,500, 2,000 and 2,500 elements with constant shape functions. The computational time of a fast and of a direct BEM solver for the 2D formulation implemented is assessed. Figure 6(a) provides a comparison of the solutions in terms of pressure directivity obtained by the fast BEM method and by the analytical solution for a distance R=50a. This solution is obtained for a cylinder discretized with 1,000 constant elements along its surface. Fifty boundary elements per box is the maximum allowed in this computation, resulting in four FMM levels. The number of terms in the FMM series that provides an accurate solution for the

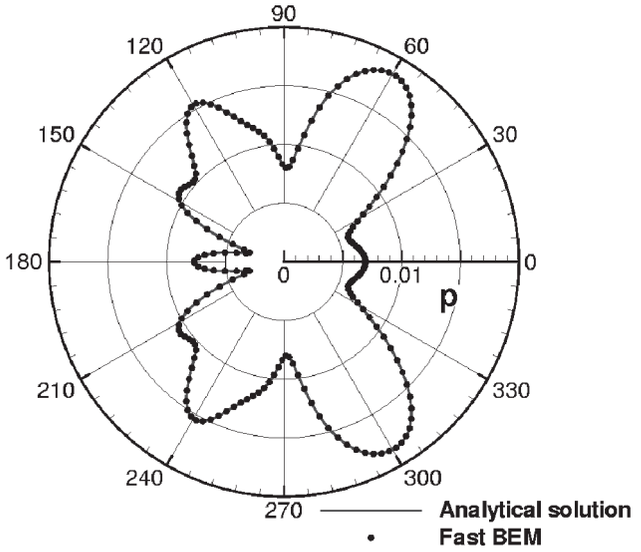

(a) 2-D cylinder

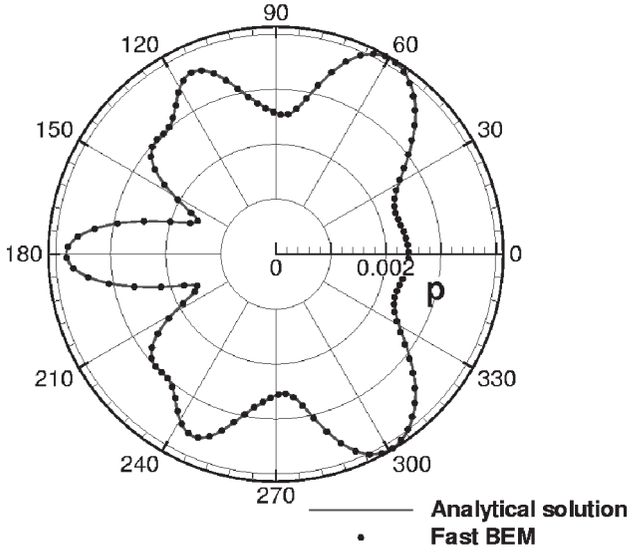

(b) Sphere

Figure 6. Pressure directivities for the acoustic scattering around a rigid cylinder and sphere for R=50a and ka=5.

wave number and dimension of the scatterer in this problem is n=4. For larger ka, this number has to be increased in order to have accurate solutions.

The convergence residue of the CGS iterative solver is set equal to 10^{-6} for all the test cases in this paper. With these conditions, the method converged in five iterations. No pre-conditioner was used to accelerate the CGS solver. One can observe that the numerical solution for pressure directivity matches perfectly with the analytical solution provided by Morris (1995a).

In Table 1, there are the comparisons of computational effort, including setup time, for the accelerated BEM and the direct BEM. One can observe that Rokhlin's single stage, or two-level, FMM is more expensive than the higher-level FMM and, for a small number of elements, the five-level FMM is more expensive than the three and four-level FMM. This is a consequence of the several recursive divisions and list constructions performed in this method. However, when the number of boundary elements is increased, the computational effort for the three-level FMM increases faster than for the four and five-levels FMM. For even finer meshes, the five-level FMM becomes the least expensive method showing that multistage FMM is necessary for large-scale problems. One can also observe that the computational time used in the direct BEM solution is much larger than the one in FMM solutions. While the direct BEM behaves proportional to $O(n^2)$ for the present simulations, the five-level FMM behaves proportional to $O(n)$.

Table 1. Total time (in seconds) spent by the fast multipole method with different levels and the direct BEM as a function of number of elements.

Method	1000 elem.	1500 elem.	2000 elem.	2500 elem.
Direct BEM	59.5	128.2	226.1	350.7
2 levels FMM	8.1	10.1	12.5	14.1
3 levels FMM	6.7	8.1	9.9	10.6
4 levels FMM	5.2	7.3	8.0	8.4
5 levels FMM	5.8	7.1	7.3	7.5

The second problem considers the acoustic scattering around a rigid sphere due to a spherically symmetric source. The solution for this problem is compared with the analytical solution presented by Morris (1995b). The point source is placed at a distance L from the center of the sphere. In the present computations, the distance L=1.0 m, the radius of the sphere is a=0.5 m and the wave number is k=10 m^{-1}, corresponding to a frequency of f=541.4 Hz for a speed of sound c=340.0 m/s.

For this test problem, the boundary of the sphere is discretized by four different meshes consisting of 2,400, 4,400, 6,200 and 9,600 quadrilateral elements with constant shape functions. The computational time of the fast and direct BEM solvers for the 3D formulation implemented is assessed. Figure 6(b) provides a comparison of the solutions in terms of pressure directivity obtained by the fast BEM method and by the analytical solution for a distance R=50 a. This solution is obtained for a sphere discretized with 2,400 constant elements along its surface. The maximum number of boundary elements per box is set equal to one hundred, resulting in two FMM levels. The number of terms in the FMM series is set to three in all the 3D calculations in this paper, except for the cavity problem, since we are considering low frequencies. One can observe that the numerical solution for pressure directivity matches perfectly with the analytical solution provided by Morris (1995b).

In Table 2, there are the comparisons of computational effort, including setup time, for the accelerated BEM and the direct BEM. The results in Table 2 show that the FMM requires less computational time compared to the direct BEM. We can also observe that the three-level FMM performs better than the two-level FMM for large-scale problems.

Table 2. Total time (in seconds) spent by the fast multipole method with different levels and the direct BEM as a function of number of elements.

Method	2400 elem.	4400 elem.	6200 elem.	9600 elem.
Direct BEM	346.4	1130.1	2979.1	7258.5
2 levels FMM	15.4	37.1	77.5	177.08
3 levels FMM	19.8	32.5	45.4	70.2

Figure 7 shows the results of a benchmark study comparing order of accuracy and memory usage of the direct and the fast BEM. The results are obtained for the acoustic scattering around the sphere previously analyzed. Three levels of adaptive refinement are used in the fast BEM solutions. The L_2 norm of the error, defined as $|E|_2 = 1/J\sqrt{\sum_{j=1}^{J} |p_j - \bar{p}_j|^2}$, is plotted as a function of the mesh refinement in a log-log plot in Fig 7(a). In the definition of $|E|_2$, p is the acoustic pressure computed by the numerical method and $\bar{p}$ is that calculated using the analytical solution. As expected, one can see that both the direct and the fast BEM achieve first order of accuracy. The error in the fast BEM solution is only slightly higher

than the equivalent for the direct BEM. This additional error can be controlled by using more terms in the truncated series or making the condition for well-separated boxes more severe, for example. However, these changes will cause the method to be more time and memory consuming. In Fig. 7(b) one can see a plot for the memory requirements for the direct and the fast BEM. In this case, the fast BEM shows a significant advantage

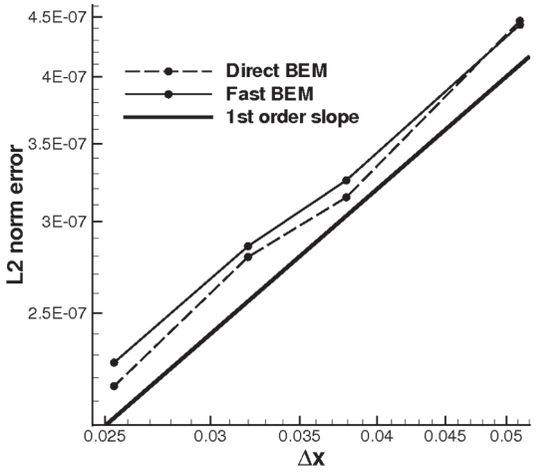

(a) L2 norm of the error

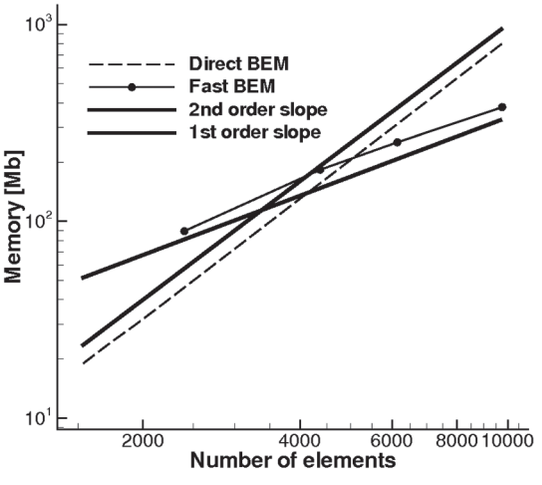

(b) Memory requirements.

Figure 7. Comparison between direct and fast BEM in terms of accuracy and memory requirements for the acoustic scattering around a sphere.

over the direct BEM in terms of memory usage for large-scale problems. Direct BEM formulations scale proportional to order $O(n^2)$ in terms of memory requirements, while the fast BEM scales proportional to $O(n)$, where n is the number of boundary elements used in the discretization.

Cylinder with cavity

The third test case presents results for the scattering of pressure waves around a rigid cylinder with a cavity, due to a monopole source located non-symmetrically with respect to the cavity. In Fig. 8(a), one can observe the 3D geometry and the mesh with 9,500 boundary elements used in this problem, and in Fig. 8(b), the pressure around the surface of the cylinder is plotted for a wave number k=10 m^{-1}. The radius of the cylinder is a=0.5 m, its length is L=1.4 m, the cavity depth is h=0.15 m, its width is d=0.2 m and its length is l=0.8 m.

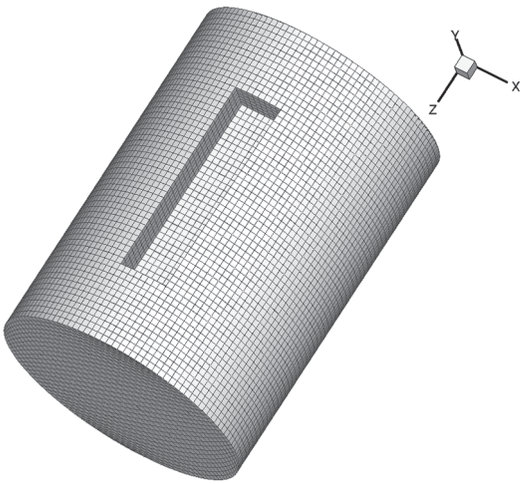

(a) Mesh with 9500 boundary elements.

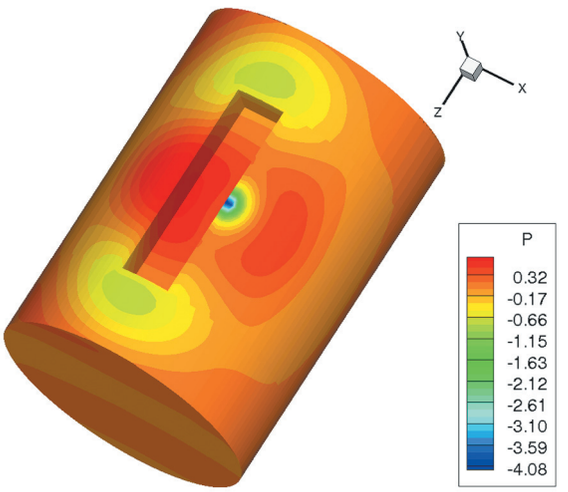

(b) Surface pressure.

Figure 8. Acoustic scattering around a rigid cylinder with a cavity due to a monopole source located non-symmetrically with respect to the cavity for ka=5.

Figure 9(a) shows the pressure field for the 3D computations obtained with a mesh of 9,500 boundary elements. In Fig. 9(b), one can see the solution for the same problem, but for a cylinder with no cavity. The source location is x = 0.1 m, y = 0.5 m, z = 0.0 m with respect to the center of the cylinder, located on the origin of the Cartesian system. We can observe the strong influence of the cavity in the scattering of the pressure waves. For the cavity case, the scattering has a preferential direction, which is from the left corner of the cavity to the source. The solutions obtained for the cylinder with no cavity show the expected symmetric scattering with respect to the source position. The effects of the cavity on the scattering of pressure waves can be observed in Fig. 10 in plots of pressure directivity for a far-field observer at a radial distance R=100 m for z=0.0 m. This figure shows results for direct and fast BEM computations, and they are in perfect agreement with each other. Again, it is possible to see the effects of the cylinder with cavity compared to the one with no cavity. The pressure directivity for the former clearly shows the preferential scattering direction. The spatial effects can also be observed, and one sees that the pressure magnitudes for the 2D calculations are larger than for the 3D, as expected. For the 2D cavity configuration, far-field pressure is smaller than that for the cylinder in all directions. For the 3D case, one can observe higher far-field pressures for angles between 0º and 90º and for 270º.

The 3D direct BEM and the two, three, and four-level FMM are compared in terms of computational time in Table 3. The time spent by each method for achieving the desired convergence is in 40 iterations. For this test case, four terms are used in the truncation of FMM series to obtain accurate results. The

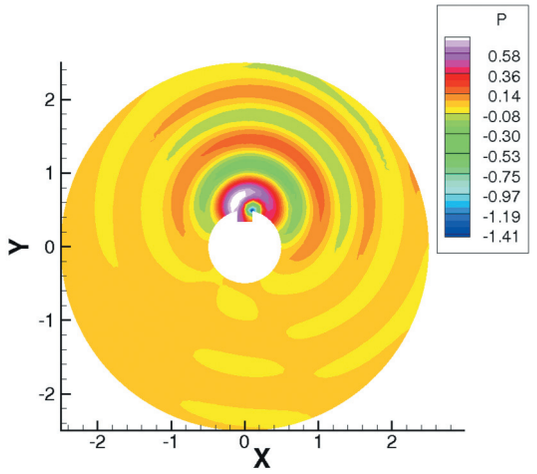

(a) Field pressure for the 3-D cylinder with cavity.

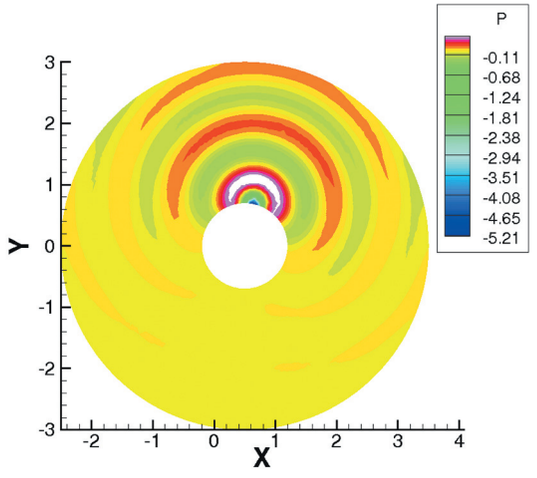

(b) Field pressure for the 3-D cylinder without cavity.

Figure 9. Acoustic scattering around a 3D rigid cylinder with a cavity due to a monopole source located non-symmetrically with respect to the cavity for ka=5.

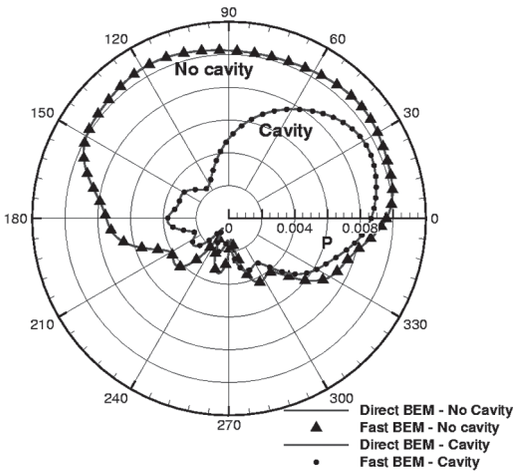

(a) 2-D simulations.

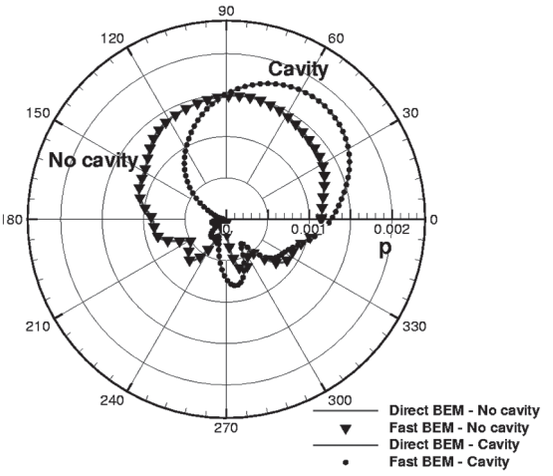

(b) 3-D simulations.

Figure 10. Pressure directivity for direct and fast BEM for a far-field with radial distance R=100 m for z=0.0.

direct BEM solution requires 49265.7 seconds for reaching the required convergence while the two, three and four-level FMM achieve convergence in 449.3, 271.1, and 299.0 seconds, respectively. The optimum number of levels of refinement is three as one can observe. For this test case, to use four levels of adaptive refinement one should set the maximum number of elements per box equal to 30, causing the FMM to be more costly than the three-level FMM. The number of elements per box should be always chosen to increase the performance of the method. It can neither be too small (many box divisions, multipole computations and translations) nor too big (many direct computations). The solution obtained with the FMM-BEM is 181 times faster than the direct BEM for the most efficient case.

Multiple bodies

The fourth studied problem assesses the implemented capability in dealing with the scattering of pressure waves around multiple bodies. A monopole source is placed at coordinates x=0.5 m, y=0.0 m on the side of two rigid cylinders in 2D or two rigid spheres in 3D. These have centers on x=0.0 m and y=±0.25 m and radius a=0.15 m. For the sphere centers, z=0.0 m. In Fig.11(a), one can observe the 3D geometry and the mesh with 10,300 boundary elements used in this problem, and in Fig.11(b), the pressure around the surface of the spheres is plotted for a wave number k=40 m^{-1}. Figs. 12(a) and (b) show plots of pressure directivity for 2D and 3D computations for a far-field with radial distance R=100 m for z=0.0 m, and the 3D relieving effects can be observed. The direct and fast BEM results are in perfect agreement as one can see in Figs. 12(a) and (b).

The 3D direct BEM and the two, three, four, and five-level FMM are compared in terms of total computational time in Table 3. One can observe the total time, including the setup one, spent by each method for achieving the desired convergence, obtained in five steps by all the schemes. The maximum number of elements per box was set as 1,000 for the two-level FMM, 300 for the three-level FMM, 100 for the four-level FMM and 50 for the five-level FMM. These are the values for best performance for each level for this test case. In this problem, the elements are more uniformly distributed inside the computational box if compared with the cavity test case. This reduces the effect of the adaptive refinement, since the computational box is refined more uniformly. As one can see in the results from Table 3, the two-level FMM is still very expensive compared to the higher level FMM, due to the many direct evaluations in the method. The optimal solution in terms of computational cost is achieved by the five-level FMM. For this number of levels of refinement, the results show a reduction in computational cost of 84 compared with direct computations.

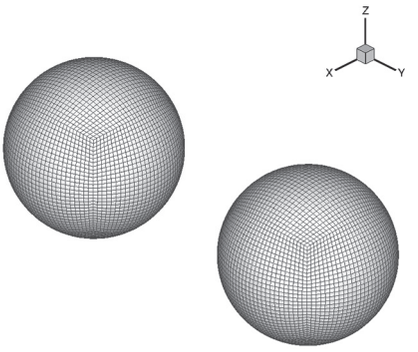

(a) Mesh with 10300 boundary elements.

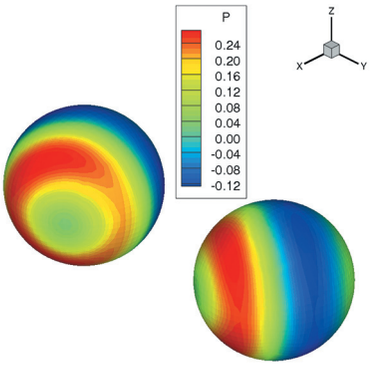

(b) Surface pressure.

Figure 11. Acoustic scattering around two rigid spheres due to a monopole source for ka=6.

Table 3. Total time (in seconds) spent by the fast multipole method with different levels and the direct BEM as a function of number of elements.

Method	Cavity (9500 el.)	Mult. Spheres (10300 el.)	Wing (14900 el.)
direct BEM	49265.7	5697.6	27706.8
2 levels FMM	449.3	3685.6	8830.4
3 levels FMM	271.1	151.1	683.5
4 levels FMM	299.0	69.0	182.2
5 levels FMM	-	67.5	137.9

Multi-element wing

This test case consists of acoustic scattering around a multi-element wing. The geometry studied is the same as in Case A-2 in the AGARD Advisory Report No. 303.40 (Moir, 1994). The airfoil configuration is comprised of a slat, main airfoil, and single-slotted flap. The slat is positioned at an angle of 25º. The flap is referred to as configuration T2 – a single slotted flap with a deflection angle of 20º, which is

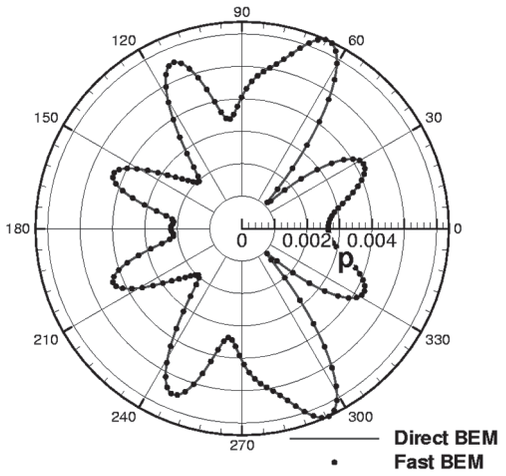

(a) Pressure directivity for the 2-D case.

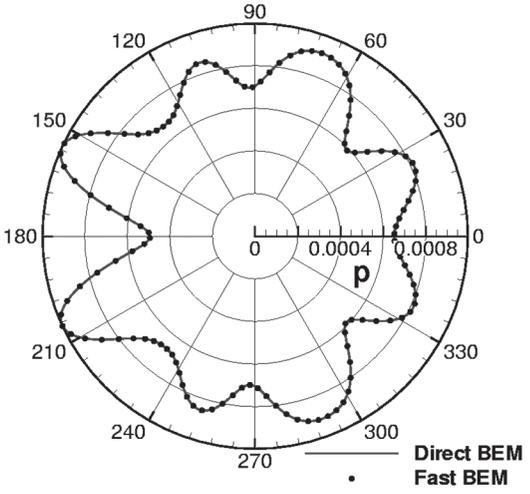

b) Pressure directivity for the 3-D case.

Figure 12. Acoustic scattering around two rigid cylinders (2D) and spheres due to a monopole source for ka=6.

(a) Mesh with 14900 boundary elements.

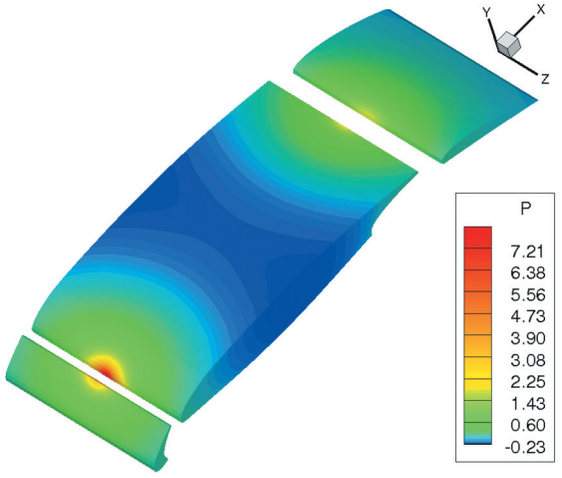

(b) Surface pressure.

Figure 13. Acoustic scattering around a multi-element wing due to two monopole sources for kc≈5.

typical of an aircraft in take-off configuration. For this case, two monopole sources are placed in the gaps formed between main airfoil and slat and flap. Figure 13(a) shows the geometry and mesh with 14,900 boundary elements analyzed in the 3D case and Fig. 13(b) shows the acoustic pressure plotted along the multi-element wing surface for a wave number k=5.0.

Figure 14 shows the pressure field for the 3D computation and a plot of pressure directivity for a far-field observer at radial distance R=100 m for z=0.0 m. The direct and fast BEM results are in perfect agreement as one can see in Fig. 14(b) for the pressure directivity plots.

The 3D direct BEM and the two, three, four, and five-level FMM are compared in terms of computational time in Table 3. One can observe the time spent by each method for achieving the desired convergence, obtained with ten steps by all the schemes. The maximum number of elements per box was set as 1,700 for the two-level, 600 for the three-level, 250 for the four-level, and 100 for the five-level FMM. As one can see in the results from Table 3, the two-level FMM is still very expensive compared to the higher level FMM, due to the many direct evaluations in the method. The three-level FMM shows a high improvement over the two-level FMM, but it is still expensive compared to the four and five-level FMM. The optimum number of refinement levels for this test case is five. For this number of levels of refinement, the results show a reduction in computational cost of 200 compared with

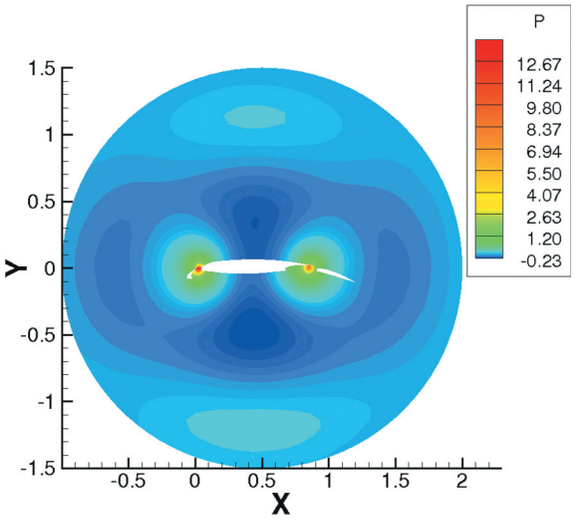

(a) Field pressure for the 3-D case for z = 0 plane.

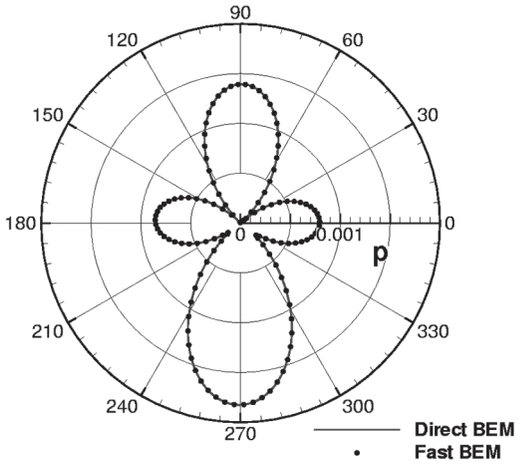

(b) Pressure directivity for the 3-D case.

Figure 14. Acoustic scattering around a multi-element airfoil due to two monopole sources for kc≈5 based on the total airfoil chord length.

direct computations. In this problem, the elements are concentrated in the center of the computational box in the y=0 plane. Therefore, the adaptive FMM works more efficiently because the scattering bodies occupy a specific region of the computational box. Thus, smaller boxes are concentrated only in the central portion of the computational box causing the FMM to have a smaller number of operations compared to cases where the scattering body is more uniformly distributed around the computational box. This occurs because there is a large number of empty boxes distant from the center of the computational box, which are forgotten when the lists are built.

CONCLUSIONS

The present work concerns the study of sound scattering from rigid bodies due to localized sources. The non-homogeneous Helmholtz equation is solved using a boundary integral formulation discretized by the BEM, which is accelerated by a multistage adaptive FMM. The Burton-Miller formulation is implemented to deal with the non-uniqueness problems of BEM for external acoustics analyses. A method that requires only regular Gaussian quadrature is presented for the solution of the hyper-singular integrals appearing in the equations. BEM calculations are attractive since their pre-processing is easier, and the equations are discretized along the boundaries only. However, for large-scale problems, the costs for solving the matrix-vector products arising from the method become prohibitive. With the acceleration provided by the FMM, boundary element calculations can be performed efficiently for large-scale problems.

For the problems analyzed in this work, the FMM-BEM provides excellent results matching analytical solutions from well-known test cases from literature. Complex geometries are studied and the fast BEM solutions are in perfect agreement with direct BEM ones. Comparisons of computational time are shown and the multistage algorithm has proved to be more efficient than the single-stage one. The results show that to have a better efficiency for an increasing number of boundary elements in the discretization, more levels are required by the FMM. However, there is always an optimum number of levels of refinement depending on the number of boundary elements and the spatial distribution of the scattering body. For boundary elements uniformly distributed over the computational box, the improvements in computational cost achieved with the adaptive refinement are lower. When the spatial distribution of the boundary elements is concentrated over a specific region of the computational box, *e.g.*, a wing located along the center of the box, the results show larger improvements in the performance of the FMM due to the adaptive refinement. In all cases, FMM-BEM reduces the computational cost relative to direct BEM. For several test problems, a factor of two orders of magnitude reduction in the cost is observed (181 for the cavity case, 84 for the multiple spheres, and 200 for the wing). In addition, FMM-BEM also reduces the memory requirement for large-scale problems.

ACKNOWLEDGEMENTS

The authors acknowledge the support of Fulbright and CAPES through a PhD Scholarship for the first author under the Fulbright/CAPES Grant No. 2464055.

REFERENCES

Brandão, M. P., 1987, "Improper Integrals in Theoretical Aerodynamics: The Problem Revisited," AIAA Journal, Vol. 25, pp. 1258-1260.

Burton, A. J., Miller, G. F., 1971, "The Application of Integral Equation Methods to the Numerical Solution of some Exterior Boundary-Value Problems," Proceedings of the Royal Society of London, Series A, Vol. 323, pp. 201-210.

Carrier, J. *et al*., 1988, "A Fast Adaptive Multipole Algorithm for Particle Simulations," SIAM Journal on Scientific and Statistical Computing, Vol. 9, No. 4, pp. 669-686.

Chen, J. T., Chen, K. H., 2003, "Applications of the Dual Integral Formulation in Conjunction with Fast Multipole Method in Large-Scale Problems for 2D Exterior Acoustics," Engineering Analysis with Boundary Elements, Vol. 28, pp. 685-709.

Cheng, H., *et al*., 1999, "A Fast Adaptive Multipole Algorithm in Three Dimensions," Journal of Computational Physics, Vol. 155, pp. 468-498.

Cheng, H., *et al*., 2006, "An Adaptive Fast Solver for the Modified Helmholtz Equation in Two Dimensions," Journal of Computational Physics, Vol. 211, pp. 616-637.

Chien, C. C., *et al*., 1990, "An Effective Method for Solving the Hypersingular Integral Equations in 3-D Acoustics," Journal of Acoustic Society of America, Vol. 88, pp. 918-937.

Darve, E., 2000, "The Fast Multipole Method I: Error Analysis and Asymptotic Complexity," SIAM Journal on Numerical Analysis, Vol. 38, No. 1, pp. 98-128.

Darve, E., Have P., 2004, "Efficient Fast Multipole Method for Low-Frequency Scattering," Journal of Computational Physics, Vol. 197, pp. 341-363.

Delnevo, A., *et al*., 2005, "Numerical Methods: Fast Multipole Method for Shielding Effects," Proceedings of the 11th AIAA/CEAS Aeroacoustics Conference, AIAA Paper 2005-2971, pp. 1-9.

Dunn, M. V., Tinetti, A. F., 2004, "Aeroacoustic Scattering Via the Equivalent Source Method," Proceedings of the 10thAIAA/CEAS Aeroacoustics Conference, AIAA Paper 2004-2937, pp. 1-11.

Epton, M. A., Dembart, B., 1995, "Multipole Translation Theory for the Three-Dimensional Laplace and Helmholtz Equations," SIAM Journal on Scientific Computing, Vol. 16, No. 4, pp. 865-897.

Geng, P., *et al*., 1996, "Massive Parallel Computation for Acoustical Scattering Problems Using Boundary Element Methods," Journal of Sound and Vibration, Vol. 191, pp. 145-165.

Greengard, L., Rokhlin, V., 1987, "A Fast Algorithm for Particle Simulations," Journal of Computational Physics, Vol. 73, pp. 325-348.

Gumerov, N. A., Duraiswami, R., 2003, "Recursions for the Computation of Multipole Translation and Rotation Coefficients for the 3-D Helmholtz Equation," SIAM Journal on Scientific Computing, Vol. 25, No. 4, pp. 1344-1381.

Jones, D. S., 1974, "Integral Equations for the Exterior Acoustic Problem," The Quartely Journal of Mechanics and Applied Mathematics, Vol. 27, pp. 129-142.

Labreuche, C., 1998, "A Convergence Theorem for the Fast Multipole Method for 2 Dimensional Scattering Problems," Mathematics of Computation, Vol. 67, No. 222, pp. 553-591.

Li, S., Huang, Q., 2011, "A Fast Multipole Boundary Element Method Based on the Improved Burton-Miller Formulation for Three-Dimensional Acoustic Problems," Engineering Analysis with Boundary Elements, Vol. 35, pp. 719-728.

Liu, Y. J., Rizzo, F. J., 1992, "A Weakly Singular Form of the Hypersingular Boundary Integral Equation Applied to 3D Acoustic Wave Problems," Computer Methods in Applied Mechanics and Engineering, Vol. 96, pp. 271-287.

Messiah, A., 1981, "Quantum Mechanics," Vol. 2, North Holland.

Moir, I. R. M., 1994, "Measurements on a Two-Dimensional Aerofoil with High-Lift Devices," A Selection of Experimental Test Cases for the Validation of CFD Codes, AGARD Report No. 303, Vol. 1 and 2.

Morris, P. J., 1995a, "The Scattering of Sound from a Spatially Distributed Axisymmetric Cylindrical Source by a Circular Cylinder," Journal of Acoustic Society of America, Vol. 97, pp. 2651-2656.

Morris, P. J., 1995b, "Scattering of Sound from a Spatially Distributed, Spherically Symmetric Source by a Sphere," Journal of Acoustic Society of America, Vol. 98, pp. 3536-3539.

Nishimura, N., 2002, "Fast Multipole Accelerated Boundary Integral Equation Methods," Applied Mechanics Reviews, Vol. 55, No. 4, pp. 299-324.

Piaszczyk, C. M., Klosner, J. M., 1984, "Acoustic Radiation from Vibrating Surface at Characteristic Frequencies," Journal of Acoustic Society of America, Vol. 75, pp. 363-375.

Rokhlin, V., 1990, "Rapid Solution of Integral Equations of Scattering Theory in Two Dimensions," Journal of Computational Physics, Vol. 86, pp. 414-439.

Rokhlin, V., 1983, "Rapid Solution of Integral Equations of Classical Potential Theory," Journal of Computational Physics, Vol. 60, pp. 187-207.

Sakuma, T., Yasuda, Y., 2002, "Fast Multipole Boundary Element Method for Large-Scale Steady-State Sound Field Analysis. Part I: Setup and Validation," Acta Acustica – Acustica, Vol. 88, pp. 513-525.

Schenck, H. A., 1968, "Improved Integral Formulation for Acoustic Radiation Problems," Journal of Acoustic Society of America, Vol. 44, pp. 41-58.

Seybert, A. F., Rengarajan, T. K., 1987, "The Use of CHIEF to Obtain Unique Solutions for Acoustic Radiation Using Boundary Integral Equations," Journal of Acoustic Society of America, Vol. 81, pp. 1299-1306.

Shen, L., Liu, Y. J., 2007, "An Adaptive Fast Multipole Boundary Element Method for Three-Dimensional Acoustic Wave Problems Based on the Burton-Miller Formulation," Computational Mechanics, Vol. 40, pp. 461-472.

Sonneveld, P., 1989, "CGS, a Fast Lanczos-type Solver for Nonsymmetric Linear Systems," SIAM Journal on Scientific and Statistical Computing, Vol. 10, pp. 36-52.

Tinetti, A. F., Dunn, M. V., 2005, "Aeroacoustic Noise Prediction Using the Fast Scattering Code," Proceedings of the 11th AIAA/CEAS Aeroacoustics Conference, AIAA Paper 2005-3061, pp. 1-12.

Tinetti, A. F., *et al*., 2007, "Curved Duct Noise Prediction Using the Fast Scattering Code," Proceedings of the 13th AIAA/CEAS Aeroacoustics Conference, AIAA Paper 2007-3528, pp. 1-15.

Wolf, W. R., Lele, S. K., 2010, "Fast Acoustic Scattering Simulations with Non-Uniform Potential Flow Effects," Proceedings of the 16th AIAA/CEAS Aeroacoustics Conference, AIAA Paper 2010-3712, pp. 1-12.

Wolf, W. R., Lele, S. K., 2009, "Assessment of Fast Multipole Method Formulations for Acoustic Scattering," Proceedings of the 15th AIAA/CEAS Aeroacoustics Conference, AIAA Paper 2009-3229, pp. 1-19.

Wu, H., *et al*., 2011, "Diagonal Form Fast Multipole Boundary Element Method for 2D Acoustic Problems Based on Burton-Miller Boundary Integral Equation Formulation and its Applications," Applied Mathematics and Mechanics, Vol. 32, pp. 981-996.

Wu, H., *et al*., 2012, "A Fast Multipole Boundary Element Method for 3D Multi-Domain Acoustic Scattering Problems Based on the Burton-Miller Formulation," Engineering Analysis with Boundary Elements, Vol. 36, pp. 779-788.

Yoshida, K, 2001, "Applications of Fast Multipole Method to Boundary Integral Equation Method," PhD. Thesis, Department of Global Environment Engineering, Kyoto University, Japan.

Yasuda, Y., Sakuma, T., 2002, "Fast Multipole Boundary Element Method for Large-Scale Steady-State Sound Field Analysis. Part II: Examination of Numerical Items," Acta Acustica – Acustica, Vol. 88, pp. 513-525.